JGR Space Physics

RESEARCH ARTICLE
10.1029/2020JA028609

Why Do Equatorial Plasma Bubbles Bifurcate?

A. J. Carrasco[1,2], A. A. Pimenta[2], C. M. Wrasse[3], I. S. Batista[2], and H. Takahashi[3]

[1]Physics Department, University of Los Andes, Mérida, Venezuela, [2]Heliophysics, Planetary Science and Aeronomy Division, National Institute for Space Research - INPE, São José dos Campos, Brazil, [3]Space Weather Division, National Institute for Space Research - INPE, São José dos Campos-SP, Brazil

Key Points:
- Several hypotheses have been proposed to explain the bifurcation observed in plasma bubbles
- Simulation results are used to study the bifurcation phenomenon observed in plasma bubbles
- The results show that the bifurcation of the plasma bubble is initiated when $E_z/E_x = 1$

Correspondence to:
A. J. Carrasco,
layerf2@gmail.com

Citation:
Carrasco, A. J., Pimenta, A. A., Wrasse, C. M., Batista, I. S., & Takahashi, H. (2020). Why do equatorial plasma bubbles bifurcate? *Journal of Geophysical Research: Space Physics*, *125*, e2020JA028609. https://doi.org/10.1029/2020JA028609

Received 20 AUG 2020
Accepted 13 OCT 2020
Accepted article online 29 OCT 2020

Author Contributions:
Writing – original draft: A. J. Carrasco
Writing – review & editing: A. A. Pimenta, C. M. Wrasse, I. S. Batista, H. Takahashi

Abstract Ionospheric plasma bubble observations using all-sky airglow imagers in the OI 630-nm emission show bifurcations with complex patterns. Bifurcation is the division of one channel of the plasma bubble into two that grow vertically in the magnetic equator. Several theories have been suggested to explain the bifurcation mechanism. In this work we use a plasma bubble simulation code to examine these theories. The model used shows that the height where the bifurcation occurs is conditioned by the polarization electric fields inside the bubble. The numerical simulation produced plasma bubbles with complex ramifications which agree with the observations taken at São João do Cariri (7.4°S, 36.5°W).

1. Introduction

Equatorial ionospheric plasma depletions, sometimes called equatorial plasma bubbles, are narrow east-west channels of updrifting plasma which are initiated by instability in the bottomside F-region of the equatorial ionosphere. In the bottomside F-region, the gravitational force and density gradient are anti-parallel, resulting in the Rayleigh-Taylor instability. The dynamic and evolution of density depletion regions or plasma bubbles within the post-sunset can lead to very complex structures. One of the outstanding problems associated with plasma bubble development is the bifurcation mechanism. The bifurcation is the division of one channel into two in a plasma bubble that grows vertically. Several branches can emerge during vertical growth. This structure is similar to a tree passing in front of the field of view of an all-sky imager. The bifurcation phenomenon has been poorly treated in the literature, and some authors agree that its cause is not yet completely understood. Nevertheless, several hypotheses have been proposed to explain the bifurcation observed in plasma bubbles (Aggson et al., 1996; Huang & Kelly, 1996d; Hysell, 1999; McDonald et al., 1981; Yokoyama et al., 2014; Zalesak et al., 1982).

According to McDonald et al. (1981), the bifurcation observed in barium clouds by simulation depends on the value of a parameter M used in their model for barium clouds. The parameter M is defined as the ratio of the field line-integrated Pedersen conductivity outside and inside the cloud. When the ratio is in the range 2–10, the bifurcation tendency is high. This result was used by Zalesak et al. (1982) to try to explain the bifurcation observed in simulation of plasma bubbles. Huang and Kelley (1996d) found that the bifurcation depends on the east-west scale size of the bubble: the bubbles bifurcate if the east-west scale size is large, but they do not bifurcate if the east-west scale size is small. Hysell (1999) studied the bifurcation based on an eigenmode analysis of plumes observed in radar images obtained with the Jicamarca radar, and he suggested that the bifurcation could occur if the appropriate superposition of instabilities exists in the bottomside of the F-region. These hypotheses will be described in detail in the next section.

In recent years, numerical modeling has been a popular tool to study the electrodynamics of equatorial plasma bubbles. In this paper, we examine the different hypotheses proposed for a plasma bubble bifurcation using an equatorial bubble simulation code in two dimensions (PBM2D). To simulate the bubble the code uses the Rayleigh-Taylor instability process. The Rayleigh-Taylor instability process was first suggested as a physical mechanism for generation of Spread-F by Dungey (1956). A first version of the PBM2D code was used by Carrasco et al. (2014), to describe the conditions of growth of the plasma bubbles at the equator over Brazilian sector and extended for low latitudes by Carrasco et al. (2017). In this work, we suggest a new mechanism to explain the bifurcation based on the results obtained with an updated version of PBM2D.

2. Observations and Theoretical Considerations

The first observational evidence of bifurcated bubbles was obtained from airglow images in the OI 630-nm emission, taken on Ascension Island (7.9°S, 14.4°W) in 1981 and reported by Anderson and Mendillo (1983). One of the manifestations of plasma bubbles in the all-sky images is a reduction in 630-nm airglow intensity as compared with the surrounding regions. The OI 630-nm emission is produced in the bottomside of the F-region (220–300 km) by the dissociative recombination process $O_2^+ + e \rightarrow O + O^*(^1D)$, with spontaneous photoemission by the excited oxygen atoms $O^*(^1D) \rightarrow O + h\nu(630\ \text{nm})$ and is widely used to monitor important ionospheric processes at F-region heights.

The use of all-sky optical imaging systems has been especially useful in studying the spatial extent of bubbles and their motion relative to the ground and to the surrounding ambient ionosphere. These airglow depletions delineate regions of reduced electron density which constitute the bubble. Pimenta (private communication) studied the occurrence of the bifurcations in 630-nm airglow images using an imaging system operated at Cachoeira Paulista (22.4°S, 45.0°W) from January 1989 to October 1991 and January 1995 to December 1997. According to Pimenta (private communication, 10 February, 2020), the occurrence of bifurcated bubbles is higher during the period of high solar activity than that of the low solar activity. As it is known, the variation of solar activity within the solar cycle causes several variations in the bubble formation. In the low solar activity period the ambient F-region plasma densities are low, and the prereversal enhancement in the vertical plasma drifts is small; the plasma is less likely to be unstable due to the low level of the Rayleigh-Taylor instability and the bubble less likely to develop. With increased solar activity, when a plasma bubble does form, its upward drift is faster, and the plasma bubble rises to higher altitude.

Figure 1 shows three examples of images obtained in 630-nm emission by the all-sky camera installed at São João do Cariri (7.4°S, 36.5°W). The circle of the images covers a diameter of approximately 1,800 km. The width of the bubble is different in each event from narrow to wide. In all cases bifurcated plasma structures can be observed. The bubble at Figure 1a shows small branches before the main bifurcation point. In Figure 1b note that the central bubble has three bifurcation points indicated by open circles. The structure at Figure 1c shows only one bifurcation point, and it is the widest bubble compared to the other two images. The observations obtained with all-sky imagers showed that generally, the bifurcation can have the shape of letter "Y" or of the letter "U." The density inside the bubble is one order of magnitude below the background value of approximately $10^5\ \text{cm}^{-3}$ (Aggson et al., 1996). The images in Figure 1 are important for comparison with the numerical results that will be presented in the following sections.

Figure 2 shows the integrated Pedersen conductivity profile between 19 and 21 LT over Brazilian sector for the moderate solar flux conditions. For the ambient plasma density along the magnetic field line the International Reference Ionosphere (IRI) model (Bilitza et al., 2016) was used. This profile will be used for the interpretation of the simulation results.

As can be seen in Figure 1 the plasma bubble structure may show complex branching patterns which depend on the geophysical conditions. Some of the existing hypotheses that attempt to explain the branching of the bubbles will be described in the following subsections.

2.1. Theory 1: The Ratio of the Integrated Pedersen Conductivity

The bifurcation mechanism studied by McDonald et al. (1981) was based on two-dimensional simulation of barium clouds. They used a parameter M defined as the ratio of the field line-integrated Pedersen conductivity outside and inside the cloud. The simulation was conducted for M values ranging from 2 to 30. The results showed that when M is moderate, in the range 2–10, the bifurcation tendency is high, while for values of M higher than 10, the tendency for the cloud to bifurcate is low. These results were hypothesized by Zalesak et al. (1982) and accepted that the same process should occurs in plasma bubbles rising into reduced conductivity regions in the upper ionosphere. In a first simulation by Zalesak et al. (1982), the bifurcated plasma bubble has the form of letter U. The rising bubble begins to flatten near the F2 peak (≈450 km) and subsequently bifurcates as it moves to higher altitude. Zalesak et al. (1982) attributed the bifurcation to the fact that the ratio of the conductivity was less than 10 in their simulated bubble. However, when they added a zonal wind to the simulation, the rising bubble began tilting westward and did not bifurcate. They suggested that the absence of bifurcation in the case with wind could be attributed to the spatial resolution used in the model simulation and that this does not allow the development of secondary instabilities from the top of the

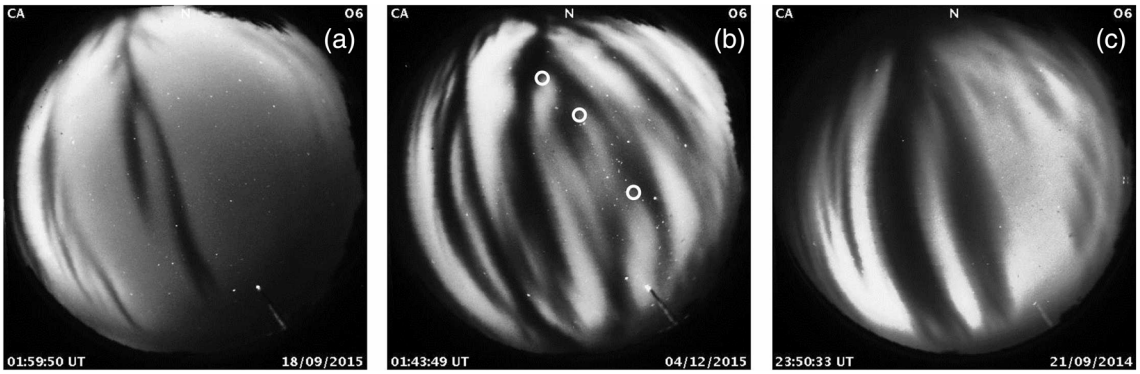

Figure 1. Airglow 630-nm images obtained at São João do Cariri on 18 September 2015 (a), 4 December 2015 (b), and 21 September 2014 (c). The diameter of the image is ~1,800 km. (Courtesy: EMBRACE Program/Brazil).

bubble. Based on these, it is possible to conclude that the ratio of the field line-integrated Pedersen conductivity outside and inside the bubble, M, could be seen as a characteristic of the bifurcated plasma bubble, but cannot physically explain why some bubbles are divided into two branches while others shown multiple bifurcations. The phenomenon of barium clouds is totally different from the physics that concerns plasma bubbles. Keskinen et al. (1998) used the three-layer model of Zalesak et al. (1982) and concluded that decreasing the background Pedersen conductivity with altitude tends to reduce the probability of a bubble to bifurcate. However, this argument is not consistent with the model results obtained by other authors (Huang & Kelley, 1996a, 1996c; Huba et al., 2015; Retterer, 2010; Yokoyama et al., 2014), which show that equatorial plasma bubble can bifurcate with conductivity decreasing with altitude. According to Anderson and Mendillo (1983), the ratio M can be calculated as follows: if an equatorial plasma bubble originates at 300 km and subsequently drifts upward to 600 km, the ratio is $M = \mathbf{\Sigma}_{600}/\mathbf{\Sigma}_{300}$, where $\mathbf{\Sigma}$ is the integrated Pedersen conductivity.

2.2. Theory 2: Bubble Thickness Effect

In the numerical simulation of equatorial plasma bubbles by Huang and Kelley (1996d), they found that plasma bubble bifurcate if the east-west scale size of the bubble is large ("wide bubbles"), but they do not bifurcate if the east-west scale size is small ("narrow bubbles"). Their textual explanation is as follows: for a narrow bubble, the electric field inside the bubble is almost homogeneous, and all charged particles within the bubble are driven to move up at a common velocity by the gravity and the electric field. Therefore, the narrow bubble rises upright without bifurcation. In contrast, for a wide bubble, the electric field and the movement of charged particles within the bubble are inhomogeneous. The charged particles in the middle of the wide bubble may walk (move) to the two sides while they drift up, which results in bifurcation of the bubble. However, these authors do not rule out the possibility that the absence of bifurcation in some of their simulated cases is caused by numerical processes in the method used. However, the observations obtained at the São João do Cariri (Figure 1) show narrow and wide bubbles with bifurcations. This suggests that a better understanding of the dynamics of the bubbles in observations and simulation is needed.

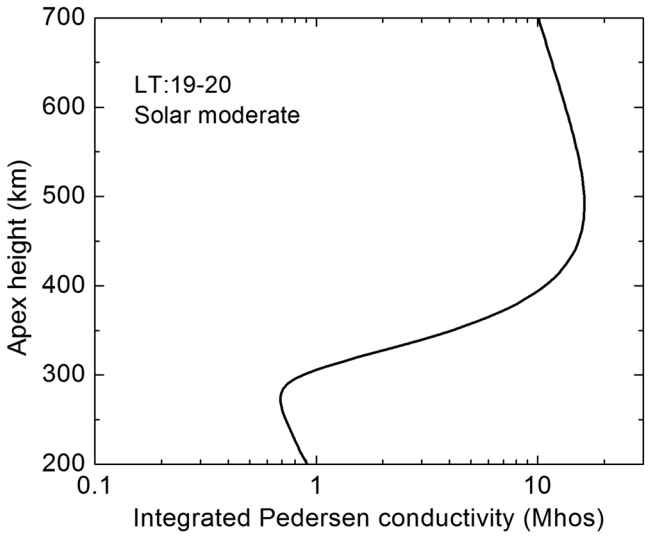

Figure 2. Pedersen conductivity profile integrated along the magnetic field line for the Brazilian sector.

2.3. Theory 3: Superposition of Eigenmode

Hysell (1999) studied the morphology of plasma irregularities based on an eigenmode analysis of plumes observed on images obtained with Jicamarca radar, and it showed evidence of secondary plasma instabilities in the bottomside of the F-region. He suggested that the bifurcation could occur if the appropriate superposition of eigenmodes exists and if the secondary instability at the leading edge of equatorial plasma bubble enters the nonlinear stage. In his study, the bifurcation was interpreted as the

growth of a secondary instability on the rising of the equatorial bubble. It is also important to comment that in a previous work, Zalesak et al. (1982) commented the possibility of secondary instabilities on the perimeters or in the interior of the bubbles, but they could not prove the hypothesis. Huang and Kelley (1996d) show that a necessary condition for production of multiple plumes is the coexistence of plasma instabilities with two different scale sizes. In fact, primary bifurcations can further bifurcate through secondary processes eventually leading to complicated patterns. In our present work, we show, for the first time, the different eigenmodes inside the bubble by simulation in section 4.

2.4. Height of the First Bifurcation

Numerical simulations of equatorial plasma bubbles have shown that the first bifurcation occurs above the density peak of the F-region (e.g., Huang & Kelley, 1996c; Retterer, 2010; Zalesak et al., 1982). After emerging on the bottomside of the F-layer, the bubble rises vertically upward. In general, once the head of the plasma bubble has passed the peak of the F-layer, the bifurcation process begins. However, Huba and Joyce (2007) showed model results of a case where the bifurcation occurred below the peak of the F-layer. This result was explained by Yokoyama et al. (2014) as being due to the two-dimensional model configuration that does not include the background E-region conductivity. The argument of Yokoyama et al. (2014) does not explain the results obtained by Huang and Kelley (1996b) using a two-dimensional model. Huang and Kelley (1996b) did not consider the conductivity of the E-region along field line, but only at the equator and, despite of that, the bifurcation occurred above the peak of the F-layer. These results show that the numerical method used for the simulation is a key point in determining the height of the bifurcation.

2.5. Electric Field Inside the Bubble

Aggson et al. (1996) utilized electric field measurements and plasma density obtained by the San Marco satellite to investigate the bifurcation of ionosphere plasma depletions at high altitudes in the equatorial region. In their analysis, a schematic illustration of the bifurcated bubble was used to interpret the satellite data. They showed that the vertical electric field inside the bubble is bipolar and varies between −3 and 6 mV/m, while the zonal component of the field varies between 1 and 13 mV/m. The measures were taken at 562 km of height when the satellite passed through an equatorial plasma bubble on 14 June 1988. According to the authors, the satellite would have passed very close to the primary bifurcation point (for more details see figure 2 of Aggson et al., 1996). As it will be discussed later, the variation of the electric field has important effects on the bifurcation mechanism.

3. Basic Equations

In recent years, numerical modeling of equatorial plasma bubbles has been a popular tool to study the electrodynamics in the equatorial ionosphere. The motion of the charged particles in the ionosphere is affected mainly by the geomagnetic field, the electric field, the gravitation, collision with neutral particles, and the pressure gradient. The equatorial ionosphere is considered in slab geometry with the Earth's magnetic field directed along the Y axis (positive northward), the gravity is in the negative Z direction, and the X axis is pointing eastward. The equations governing equatorial spread-F instability growth within the context of the collisional Rayleigh-Taylor mechanism are as follows:

$$\frac{\partial N}{\partial t} = -\beta N - \vec{\nabla} \cdot \left(N \vec{V_i} \right) \tag{1}$$

$$\vec{\nabla} \cdot \vec{J} = \vec{\nabla} \cdot \left[e \left(N_i \vec{V_i} - N_e \vec{V_e} \right) \right] = 0 \tag{2}$$

$$\frac{e}{m_i} \left(\vec{E} + \vec{V_i} \times \vec{B} \right) - \nu_i \left(\vec{V_i} - \vec{U} \right) - \frac{1}{N_i m_i} \vec{\nabla} P_i + \vec{g} = 0 \tag{3}$$

$$-\frac{e}{m_e} \left(\vec{E} + \vec{V_e} \times \vec{B} \right) - \nu_e \left(\vec{V_e} - \vec{U} \right) - \frac{1}{N_e m_e} \vec{\nabla} P_e + \vec{g} = 0 \tag{4}$$

The subscripts e and i refer to electrons and ions, respectively. In the F-region for altitude above 200 km the domination is ionized atomic oxygen. Equation 1 is the continuity equation for the ion O^+, and

Equation 2 is the divergence-free current ($\vec{J}$). $\vec{V}_i$ and $\vec{V}_e$ are the velocities for ions and electrons, respectively. $\vec{U}$ is the neutral wind velocity, m_i and m_e are the mass for ions and electrons, ν_i and ν_e are the collision frequency of ions and electrons with neutrals, β is the recombination coefficient, $\vec{g}$ is the gravitational acceleration, and P_i and P_e are the thermal pressures of ions and electrons. $\vec{E} = \vec{E}_0 - \vec{\nabla}\,\Phi$ is the electric field, $\vec{E}_0 = \vec{E}_{0x} + \vec{E}_{0z}$ is the background electric field, Φ is the perturbation electrical potential, the gradient operator is given by $\vec{\nabla} = (\partial/\partial x)\hat{i} + (\partial/\partial z)\hat{k}$, and $\vec{B}$ is the magnetic field. For simplicity the vertical electric field, which causes the zonal plasma drift, can be estimated by $E_{0z} \approx -UB$ (Anderson & Mendillo, 1983). The ionospheric plasma is assumed to be electrically neutral ($N_e = N_i = N$). Making the approximation $\nu_e/\Omega_e \ll 1$ and $\nu_e^2/\Omega_e^2 \to 0$, the equation for the electrostatic potential is given by

$$\frac{\partial^2\Phi}{\partial z^2} + \frac{\partial^2\Phi}{\partial x^2} + \frac{\partial \ln \sigma_p}{\partial z}\frac{\partial\Phi}{\partial z} + \frac{\partial \ln \sigma_p}{\partial x}\frac{\partial\Phi}{\partial x} = \left(\frac{Bg}{\nu_i} + E_{0x}\right)\frac{\partial \ln \sigma_p}{\partial x} - \frac{B}{\Omega_i}g\frac{\partial \ln \sigma_p}{\partial z} \tag{5}$$

where σ_p is the Pedersen conductivity defined as (Anderson & Mendillo, 1983; Zalesak et al., 1982)

$$\sigma_p = \frac{Ne^2}{m_i}\frac{\nu_i}{\nu_i^2 + \Omega_i^2} \tag{6}$$

The continuity Equation 1 can be rewritten as

$$\frac{\partial N}{\partial t} = -\beta N - \frac{\partial}{\partial x}(NV_x) - \frac{\partial}{\partial z}(NV_z) \tag{7}$$

The zonal (V_x) and vertical (V_z) components of the plasma velocity are given by

$$V_x = \frac{1}{1 + \nu_i^2/\Omega_i^2}\left(-\frac{E_{0z}}{B} + \frac{1}{B}\frac{\partial\Phi}{\partial z} - \frac{\nu_i}{\Omega_i B}\frac{\partial\Phi}{\partial x} + \frac{1}{\Omega_i}g\right) \tag{8}$$

$$V_z = \frac{1}{1 + \nu_i^2/\Omega_i^2}\left(\frac{\nu_i}{\Omega_i}U + \frac{E_{0x}}{B} - \frac{1}{B}\frac{\partial\Phi}{\partial x} - \frac{\nu_i}{\Omega_i B}\frac{\partial\Phi}{\partial z} - \frac{\nu_i}{\Omega_i^2}g\right) \tag{9}$$

The system of Equations 5–9 are the equations of the Plasma Bubbles Model in two dimensions (called PBM2D) for the magnetic equatorial region. Equation 6 was solved using a line by line successive over-relaxation (SOR) method. Equation 8 was solved using a predictor-corrector method with flux-corrected transport (FCT). The FCT is a technique originally developed by Boris and Book (1973) in one dimension, which we extended to two dimensions. The PBM2D is used in the present work to study the bifurcation phenomenon in equatorial plasma bubble. Note that we have neglected the pressure effects in Equations 8 and 9. We wished to show that a model that does not take into account parameters integrated along the flux tube can also explain some characteristics of the bubbles as shown by Huang and Kelley in a series of articles.

4. Numerical Results and Discussion

The main purpose of the present paper is to examine the different theories proposed on the bifurcation mechanism. In the following subsections the numerical results obtained with PBM2D are presented. For simplicity and clarity, the neutral wind is set equal to zero. The grid in PBM2D has 5-km resolution in altitude (200–700 km) and 4 km in longitude (±200 km) at the magnetic equatorial plane. An initial perturbation with wavelength of 200 km and amplitude of 5% is imposed to the background plasma density. The perturbation is centered at ±100 km of zonal distance. A background eastward electric field was applied with a value of 0.5 mV/m and a magnetic field with a value of 0.25×10^{-4} Tesla. Both fields produce a background vertical drift of 20 m/s. The system is initialized at 18:05 LT. The magnitude of the perturbation is consistent with that obtained by Carrasco and Batista (2012) at the magnetic equatorial region in Brazil. Two plasma bubbles events are modeled. The width of the simulated plasma bubbles is small when compared to the

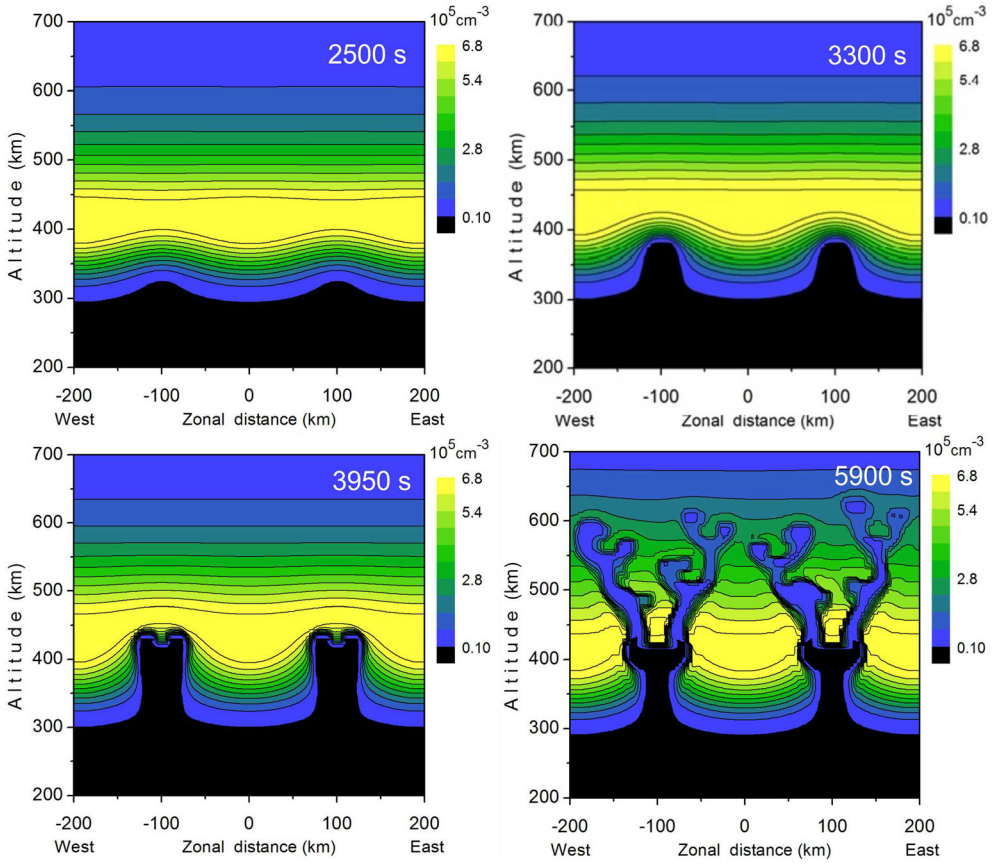

Figure 3. Contours of the electron density at four times for event 1. At time 3,950 s the bifurcation begins.

observed plasma bubbles. In general, it is accepted that the spread-F or plasma bubble is due to nonlinear evolution of the Rayleigh-Taylor instability.

4.1. Bubbles by Simulation

For the first event the ambient plasma density profile is such that the F_2 peak at time $t = 0$ s (18:05 LT) is located at 350 km and the numerical density is 9×10^5 cm^{-3}. The results are shown in Figure 3 as contour plots of electron density as a function of zonal distance and altitude at 2,500, 3,300, 3,950, and 5,900 s of evolution starting with the initial steep stage and ending with a branched structure. At time 3,300 s the initial perturbations were evolved into two bubbles at (around) ±100 km of zonal distance. At time 3,950 s the bubbles have bifurcated and have risen to over 400 km and above the density peak of the F-region (which was 350 km for this event). The bubbles continue to evolve until two more bifurcations are observed around 500 and 590 km of altitude at time 5,900 s. The midpoint of each bubble at 410 km begins to flatten and rise very slowly when compared to the two branches (left and right). At 550 km of altitude (5,900 s), the two branches of the bubbles are separated by ~130 km. This value is close to 153-km separation reported by Aggson et al. (1996). In the simulation for the present case the bubbles exhibit up to three bifurcation points in the plasma structure. The number of bifurcations is comparable with some of the events observed in São João do Cariri (see Figure 1b).

For the second event, the ambient plasma density profile is such that the F_2 peak at time $t = 0$ s (18:05 LT) is located at 430 km and the numerical peak density is 9×10^5 cm^{-3}. Figure 4 shows the evolution of the bubbles at times 3,250 and 4,200 s. At time 3,250 s the bubbles were bifurcated and rose up to over 500 km of altitude. In both events the background ratio of the field line-integrated Pedersen conductivity is calculated as follows: the plasma bubble originates at 310 km in event 1 and at 325 km in event 2. Subsequently, the plasma bubble bifurcates at ~400 km in event 1 and at ~500 km in event 2. Using Figure 2 the ratio can

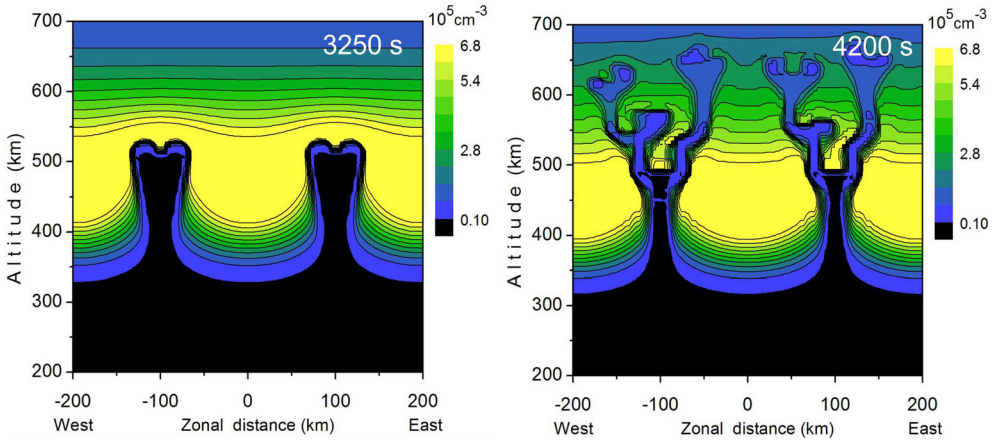

Figure 4. Contours of the electron density at two times for event 2. At time 3,250 s the bifurcation begins.

be calculated as $M = \Sigma_{400}/\Sigma_{310} = 9.6$ for event 1 and as $M = \Sigma_{500}/\Sigma_{325} = 8.8$ for event 2. Note that, in both events the ratio is less than 10. From these results we can say that, $M \leq 10$ is an inherent feature in bifurcated plasma bubbles. The comparison of both events is of importance to understand the bifurcation mechanism described in section 4.3. All simulated bubbles have a zonal width of 50 km at their base. An additional simulation (not shown here) reveals that for a bubble 100 km wide the primary bifurcation also occurs and with characteristics similar to those of Events 1 and 2.

4.2. Determination of Instability Modes in the Simulation Results

For the first time the existence of instability modes inside the bubble is studied using simulation results. To determine the superposition of modes of instabilities inside the bubble, the discrete Fourier transform (DFT) technique is applied to the series of values of plasma density, *N*. For event 1 (Figure 3), the discrete series is formed by the zonal variation of *N* at a fixed height. It is important to remark that the choice of the fixed height depends on the growth stage of the bubble. At 10 s of simulation the fixed height was 310 km which is very close to the height of the initial perturbation. For 5,900 s the fixed height was 400 km very close to the bifurcation point. Thus, when the series transform is known, one can calculate the square to obtain the power spectral density (PSD). Figure 5 shows the periodogram obtained from the series. At time 10 s we see only the fundamental mode, as expected, and at 5,900 s two additional modes are identified. The wavelengths of the modes are 200, 50, and 29 km, respectively. These results confirm the suspicion of several authors about the existence of other modes of instability inside the plasma structure. The overlapping of modes produces complex structures. Note that these results correspond to the primary bifurcation and the process can be repeated at other bifurcation points of the plasma structure. Additionally, for 525 km height (left bubble and left arm in Figure 3) the dominant mode is the one with wavelength 100 km (their PSD is not

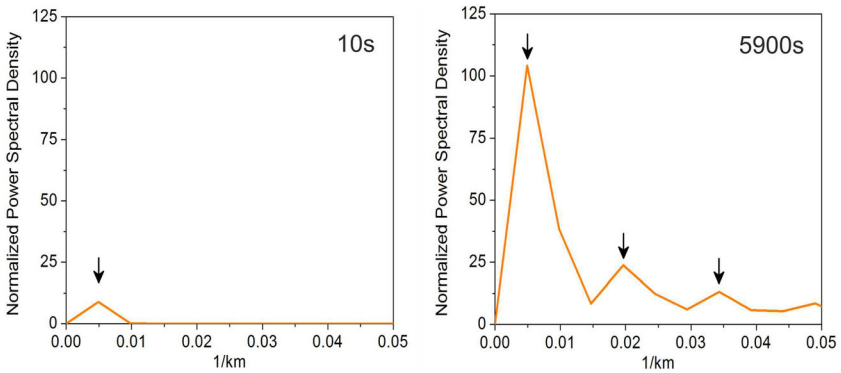

Figure 5. Plot of Fourier transform for event 1. At time 5,900 s three modes are observed.

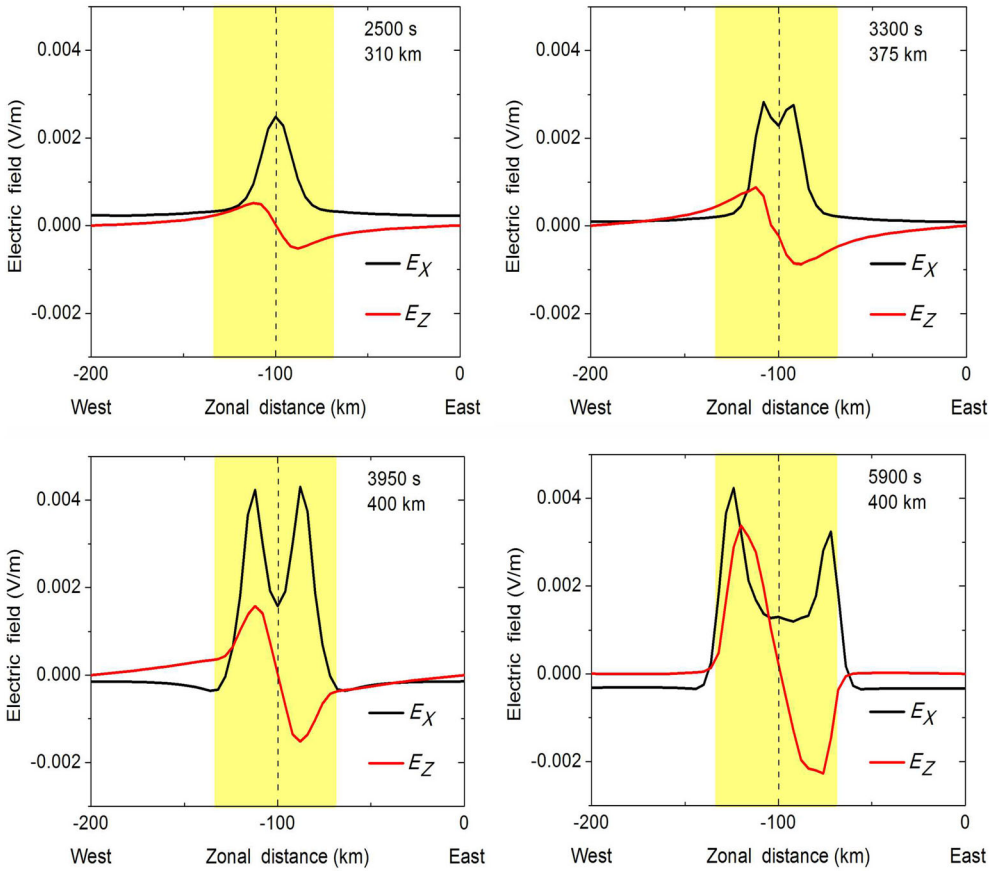

Figure 6. Plot of the zonal and vertical components electric field inside the bubble for event 1. In the graphics sequence the fields are inhomogeneous.

shown here). Based on the results, the modes can be related to the movement of the charged particles, which in turn are controlled by the polarization electric fields inside the bubbles. The polarization electric fields inside the bubble are detailed in the next subsection.

4.3. Electric Field Inside the Bubble

The polarization electric field that is generated inside the bubble can be mapped along the magnetic field lines to higher latitudes, beyond the limited density depletion structure (Weber et al., 1996). At the magnetic equatorial region the zonal electric field component (E_x), defined as positive in the eastward direction, produces an upward plasma drift, while the vertical electric field component (E_z), defined as positive upwards, produces a westward drift. In situ observations of electric field inside plasma bubbles obtained by San Marco satellite reveal a unipolar variation in E_x and a bipolar variation in E_z at 562 km altitude at the magnetic equator (Aggson et al., 1996). Figure 6 shows the variation of the electric field at a fixed height for the event 1 (Figure 3), obtained from the solution of Equation 5. In the figure the yellow-shaded column denotes the width of the bubble. At time 2,500 s E_x (black line) peaks at 0.0025 V/m, and E_z (red line) is very close to zero. At time 3,300 s the zonal field shows two peaks, and the vertical field continues to increase. At time 3,950 s the minimum value of the zonal field in the middle part of the bubble is very close to maximum of the vertical field. The effect of the fields on the particles is as follows: inside the bubble the movement of the charged particles is controlled by both drifts. Simultaneously, as the vertical drift lifts the particles, the bipolar vertical field tends to separate the flow of particles towards the walls of the bubble. The bifurcation, or the division of one channel, is initiated when the maximum of the vertical field (positive) is very close to the minimum value of the zonal field in the middle part of the bubble (see Figures 3 and 6) or in other words, for $E_z \approx E_x = 0.0015$ V/m (at 3,950 s). At time 5,900 s the minimum (valley region) in the zonal field is extended in the zonal direction and the vertical field increases.

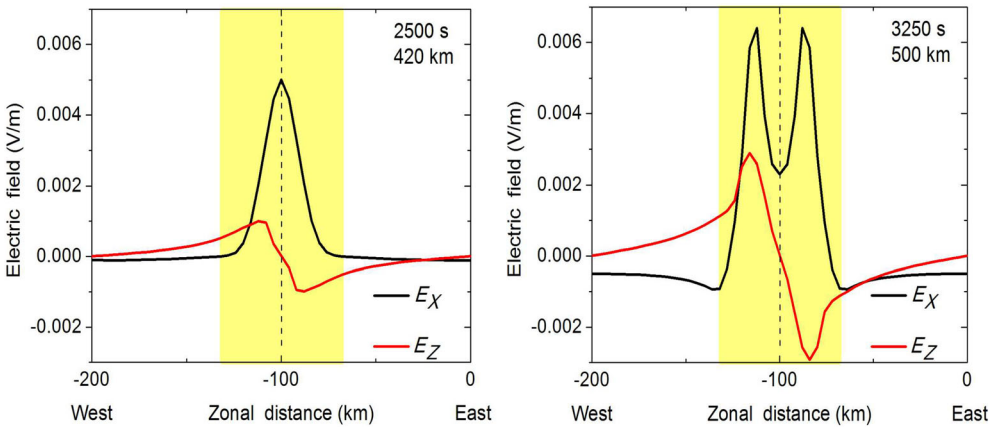

Figure 7. Plot of the zonal and vertical components of the electric field inside the bubble for event 2.

The same analysis concerning the electric field components inside the bubble was repeated for the event 2. The geophysical parameters were identical to those for the event 1 with the exception of the F_2 peak height which was located at 430 km. For the second event the bifurcation occurred at 500 km (Figure 4), and the condition $E_z \approx E_x = 0.0025$ V/m occurs at 3,250 s (Figure 7). These results demonstrate that the ratio $E_z^{\max}/E_x^{\min} = 1$ should be taken as the principal condition for the bifurcation process. The results reveal that the zonal electric field inside the bubble emerges first, followed be the vertical electric field development. The analysis of the obtained results, allow explaining in detail the bifurcation mechanism that acts on the plasma bubbles.

The bipolar variation of the vertical electric field can be understood as follows. The bipolar behavior of the vertical field is related with the configuration of the lines of the electric potential that surrounds the bubble (not shown here but its configuration published by other authors, e.g., Zalesak et al., 1982). At the midpoint of the vertical plasma structure the isolines of electric potential are vertical, but they begin to curve toward the walls (east-west). Additionally, toward the walls the isolines of electric potential are positive westward and negative eastward. In a first approximation the components of the electric field can be obtained from the electric potential by $\overrightarrow{E} = -\overrightarrow{\nabla}\,\Phi$. Where the potential, Φ, is obtained by solution of the Equation 5. For the vertical component of the field the derivate, $-\partial\Phi/\partial z$, is positive towards the west side and negative towards east side. But the derivate is zero at the midpoint where the lines are vertical. Consequently, with a magnetic field pointing northward, the vertical electric fields induce westward plasma drift at western side, and eastward plasma drift at the eastern side.

5. Conclusions

We have studied the generation and evolution of equatorial plasma bubbles using the code PBM2D. The generation, growth, and bifurcation of plasma bubbles were reproduced in the simulations. In our work the physical mechanism for the bifurcation of plasma bubbles was clarified. Our simulations show that the channel division or bifurcation of the bubble is initiated when the maximum of the vertical field (positive) is very close to the minimum value of the zonal field in the middle part of the bubble. Then the bifurcation is amplified and finally the plasma bubble branches. We have observed successive bifurcations when the bubble continues its growth. The altitude of the principal bifurcation point can vary quite considerably depending on the initial altitude of the F_2 peak. From all theories examined in this work, certainly, Huang and Kelley (1996d) was very close to explain the bifurcation conditions, but they did not identify the condition of fields, $E_z^{\max}/E_x^{\min} = 1$, presented in our model.

It is well known that after sunset the decrease of conductivity along field line allows the development of polarization fields inside the bubble. Within the context of the present simulations, the condition that the ratio of the Pedersen conductivity outside and inside the equatorial bubble should be less of 10 is a charac-

teristic of bifurcated plasma bubble but cannot physically explain why the bubble is divided into two branches.

Additionally, our simulation revealed the existence of three modes of instability that coexist inside the bubble. The existence of the modes is a consequence of the distribution of the particles, which are caused by polarization electric field inside the bubble. Furthermore, the results reveal that the zonal electric field emerges first and after a time the vertical electric field develops. It is concluded that the drift caused by the bipolar vertical electric field result in the bifurcation of the plasma bubble. Our simulations are consistent with the observations and provide new insight on branching physics in plasma structures. The influence of neutral wind on the bifurcation mechanism will be examined in future work. On the other hand, since the present simulation is restricted to the equatorial region, it was not possible to take into account the effects of the low latitude E-region conductivity via magnetic flux tube on the bifurcation mechanism. Such an effect can only be included using a field line integration model, which is not the present case. We wish to close this section, saying that the revised theories have had relevance in the results presented here.

Conflicts of Interest

The authors declare that they have no conflict of interest.

Data Availability Statement

The airglow images of São João do Cariri can be downloaded upon registration at the Embrace webpage from INPE Space Weather Program in a website (http://www2.inpe.br/climaespacial/portal/en/). The IRI program can be accessed online (http://www.irimodel.org). PBM2D calculations have been uploaded at a website (http://doi.org/10.5281/zenodo.4075587).

Acknowledgments

The authors wish to acknowledge the support from CAPES-PRINT (process 8887.374260/2019-00) through which the visit of Dr Carrasco to the National Institute for Space Research – INPE was made possible.

References

Aggson, T. L., Laakso, H., Maynard, N. C., & Pfaff, R. F. (1996). In situ observations of bifurcation of equatorial ionospheric plasma depletions. *Journal of Geophysical Research*, *101*(A3), 5125–5132. https://doi.org/10.1029/95JA03837

Anderson, D. N., & Mendillo, M. (1983). Ionospheric conditions affecting the evolution of equatorial plasma depletions. *Geophysical Research Letters*, *10*, 541–544. https://doi.org/10.1029/GL010i007p00541

Bilitza, D., Altadill, D., Truhlik, V., Shubin, V., Galkin, I., Reinisch, B., & Huang, X. (2016). International Reference Ionosphere 2016: From ionospheric climate to real-time weather predictions. *Space Weather*, *15*, 418–429. https://doi.org/10.1002/2016SW001593

Boris, J. P., & Book, D. L. (1973). Flux-corrected transport. I. SHATA, a fluid transport algorithm that works. *Journal of Computational Physics*, *11*, 38–69. https://doi.org/10.1016/0021-9991(73)90147-2

Carrasco, A., & Batista, I. S. (2012). Estimation of the initial amplitude of plasma bubble seed perturbation from ionograms. *Radio Science*, *47*, RS2008. https://doi.org/10.1029/2011RS004862

Carrasco, A., Batista, I. S., & Abdu, M. A. (2014). Numerical simulation of equatorial plasma bubbles over Cachimbo: COPEX campaign. *Advances in Space Research*, *54*, 443–445. https://doi.org/10.1016/j.asr.2013.10.017

Carrasco, A., Batista, I. S., Sobral, J. H. A., & Abdu, M. A. (2017). Spread-F modeling over Brazil. *Journal of Atmospheric and Terrestrial Physics*, *161*, 98–104. https://doi.org/10.1016/j.jastp.2017.06.015

Dungey, J. W. (1956). Convective diffusion in the equatorial F-region. *Journal of Atmospheric and Terrestrial Physics*, *9*, 304–310. https://doi.org/10.1016/0021-9169(56)90148-9

Huang, C. S., & Kelley, M. C. (1996a). Nonlinear evolution of equatorial spread F: On the role of plasma instabilities and spatial resonance associated with gravity wave seeding. *Journal of Geophysical Research*, *101*, 283–292. https://doi.org/10.1029/95JA02211

Huang, C. S., & Kelley, M. C. (1996b). Nonlinear evolution of equatorial spread F: Gravity wave, velocity shear, and day-to-day variability. *Journal of Geophysical Research*, *101*, 521–532. https://doi.org/10.1029/96JA02332

Huang, C. S., & Kelley, M. C. (1996c). Nonlinear evolution of equatorial spread F: Plasma bubbles generated by structure electric fields. *Journal of Geophysical Research*, *101*, 303–313. https://doi.org/10.1029/95JA02209

Huang, C. S., & Kelley, M. C. (1996d). Nonlinear evolution of equatorial spread F: Gravity wave seeding of Rayleigh-Taylor instability. *Journal of Geophysical Research*, *101*, 293–302. https://doi.org/10.1029/95JA02210

Huba, J. D., & Joyce, G. (2007). Equatorial spread F modeling: Multiple bifurcated structures, secondary instabilities, large density 'bite-outs', and supersonic flows. *Geophysical Research Letters*, *34*, L07105. https://doi.org/10.1029/2006GL028519

Huba, J. D., Wu, T. W., & Makela, J. J. (2015). Electrostatic reconnection in the ionosphere. *Geophysical Research Letters*, *42*, 1626–1631. https://doi.org/10.1002/2015GL063187

Hysell, D. L. (1999). Imaging coherent backscatter radar studies of equatorial spread F. *Journal of Atmospheric and Solar-Terrestrial Physics*, *61*, 701–716. https://doi.org/10.1016/S1364-6826(99)00020-6

Keskinen, M. J., Ossakow, S. L., Basu, S., & Sultan, P. J. (1998). Magnetic-flux-tube-integrated evolution of equatorial ionospheric plasma bubbles. *Journal of Geophysical Research*, *103*, 3957–3967. https://doi.org/10.1029/97JA02192

McDonald, B. E., Ossakow, S. L., Zalesak, S. T., & Zabusky, N. J. (1981). Scale sizes and lifetimes of F region plasma cloud striations as determined by the condition of marginal stability. *Journal of Geophysical Research*, *86*, 5775–5784. https://doi.org/10.1029/JA086iA07p05775

Retterer, J. M. (2010). Forecasting low-latitude radio scintillation with 3-D ionospheric plume models: 1. Plume model. *Journal of Geophysical Research*, *115*, 1–18. https://doi.org/10.1029/2008JA013840

Weber, E. J., Basu, S., Bullett, T. W., Valladares, C., Bishop, G., Groves, K., et al. (1996). Equatorial plasma depletion precursor signature and onset observed at 11° south of the magnetic equator. *Journal of Geophysical Research*, *101*, 26,829–26,838. https://doi.org/10.1029/96JA00440

Yokoyama, T., Shinagawa, H., & Jin, H. (2014). Nonlinear growth, bifurcation, and pinching of equatorial plasma bubble simulated by three-dimensional high-resolution bubble model. *Journal of Geophysical Research: Space Physics*, *119*, 10,474–10,482. https://doi.org/10.1002/2014JA020708

Zalesak, S. T., Ossakow, S. L., & Chaturvedi, P. K. (1982). Nonlinear equatorial spread F: The effect of neutral winds and background Pedersen conductivity. *Journal of Atmospheric and Terrestrial Physics*, *77*(A1), 151–166. https://doi.org/10.1029/JA087iA01p00151